Published in final edited form as:
Biochemistry. 2012 November 6; 51(44): 8791–8801. doi:10.1021/bi300954g.

Entamoeba histolytica Rho1 regulates actin polymerization through a divergent, Diaphanous-related formin

Dustin E. Bosch[1], **Bing Yang**[2], and **David P. Siderovski**[3,*]

[1]Department of Pharmacology, The University of North Carolina at Chapel Hill, Chapel Hill, NC 27599-7365 USA

[2]Department of Cell and Developmental Biology, The University of North Carolina at Chapel Hill, Chapel Hill, NC 27599-7365 USA

[3]Department of Physiology and Pharmacology, West Virginia University School of Medicine, Morgantown, WV 26506-9229 USA

Abstract

Entamoeba histolytica requires a dynamic actin cytoskeleton for intestinal and systemic pathogenicity. Diaphanous-related formins represent an important family of actin regulators that are activated by Rho GTPases. The *E. histolytica* genome encodes a large family of Rho GTPases and three diaphanous-related formins, of which EhFormin1 is known to regulate mitosis and cytokinesis in trophozoites. We demonstrate that EhFormin1 modulates actin polymerization through its formin homology 2 (FH2) domain. Despite a highly divergent diaphanous autoinhibitory domain, EhFormin1 is autoinhibited by an N- and C-terminal intramolecular interaction, but activated upon binding of EhRho1 to the N-terminal domain tandem. A crystal structure of the EhRho1·GTPγS/EhFormin1 complex illustrates an EhFormin1 conformation that diverges from mammalian mDia1 and lacks a secondary interaction with a Rho insert helix. The structural model also highlights residues required for specific recognition of the EhRho1 GTPase and suggests that the molecular mechanisms of EhFormin1 autoinhibition and activation differ from mammalian homologs.

Keywords

actin polymerization; guanine nucleotide binding protein

Entamoeba histolytica is the causative agent of amoebic colitis and systemic amoebiasis (1). Infection by the parasite is spread endemically among poor populations of developing countries, although outbreaks among travelers and susceptible populations occur in the United States (1). Water-borne *E. histolytica* cysts cycle to the trophozoite form in the human host, in some cases leading to destruction of the intestinal mucosa (amoebic colitis). If untreated, trophozoites may enter the blood stream, leading to systemic amoebiasis characterized by liver, lung, and brain abscesses (2). Many cellular processes critical to *E. histolytica* pathogenesis, such as chemotaxis, adherence to intestinal epithelium, cell killing,

*Address correspondence to Dr. David P. Siderovski, 3051 Robert C. Byrd Health Sciences Center, West Virginia University School of Medicine, Morgantown, WV 26506-9229 USA. Tel: 304-293-4991; dpsiderovski@hsc.wvu.edu.

Supplemental Information

Supporting information includes protein sequence information and constructs used in this study, supporting EhRho1/EhFormin1 fusion binding experiments, additional comparison of the EhRho1/EhFormin1 complex to previous structures, an analysis of crystal contacts, and an example electron density map. The supplemental information associated with this manuscript may be accessed free of charge online at http://pubs.acs.org.

phagocytosis, and penetration of the mucosa are dependent on a highly dynamic actin cytoskeleton (3–5). *E. histolytica* expresses a relatively large number of Rho family small GTPases (6, 7), conserved signaling molecules that are vital to coordination of actin cytoskeletal rearrangements (8). Rho GTPases undergo a conformational change dominated by switch regions upon exchange of GTP for GDP, allowing engagement of specific downstream effectors (9). Overexpression of constitutively active versions of the Rho family GTPases EhRacA or EhRacG in *E. histolytica* trophozoites impairs pathogenic processes such as phagocytosis and surface receptor capping (10, 11). However, signaling mechanisms by which the actin cytoskeleton of *E. histolytica* is regulated have not been elucidated in molecular detail.

Formins constitute a major class of proteins that directly regulate actin filament formation and thus cellular morphology, adhesion, and motility (12). Formins promote nucleation and polymerization of unbranched actin filaments (13). The highly conserved formin homology 2 domain (FH2) forms a head-to-tail dimer that binds to the barbed ends of actin filaments, catalyzing assembly through a processive capping mechanism (12, 14, 15). The FH2 domain is commonly preceded by an unstructured, proline-rich formin homology 1 domain (FH1) that engages profilin/actin complexes, thus recruiting G-actin monomers for incorporation into a growing filament (12). Members of the Diaphanous-related formin (DRF) subfamily also possess an N-terminal Rho GTPase binding domain (GBD) and a formin homology 3 domain (FH3) that, in turn, is composed of an Armadillo repeat-containing Diaphanous inhibitory domain (DID) and a dimerization domain (13). C-terminal to the FH2 domain of DRFs is a Diaphanous autoinhibitory domain (DAD) that forms intramolecular interactions with the DID, maintaining the formin in an inactive state, as best characterized structurally for the DRF mDia1 (16, 17). This autoinhibited conformation is released upon binding of specific Rho family GTPases to the GBD-FH3 domain tandem, likely due to active DAD displacement from its DID binding site by Rho-induced contingent folding of the GBD and by the Rho GTPase itself (18, 19). Although mDia1 primarily engages one of its activating GTPases, RhoC, through the switch regions, the last Armadillo repeat of the DID also weakly contacts the signature Rho insert helix of RhoC (20). Mutation of residues at this secondary interface leads to reduced RhoC/mDia1 affinity, but it is unclear whether the interaction is important for formin activation *per se* (14).

E. histolytica possesses a family of eight formins, among which EhFormin1–3 are Diaphanous-related (21). EhFormin1 and -2 are expressed in trophozoites and associated with pseudopodia, pinocytic and phagocytic vesicles, and F-actin in response to serum. Both formins are also co-localized with the microtubular assembly during mitosis (21). Overexpression of EhFormin1 increases the number of binucleated cells and nuclear DNA content, suggesting roles for EhFormin1 in mitosis and cytokinesis (21). A recent proteomic characterization of *E. histolytica* cysts indicated that EhFormin1 is expressed during both the encysted and trophozoite life cycle stages (22). We recently showed (7) that the GBD-FH3 domain tandem of EhFormin1 binds EhRho1 in a nucleotide state-dependent fashion, which is typical of Rho GTPase/effector interactions. Furthermore, expression of constitutively active EhRho1 in fibroblasts induced stress fiber formation (7), suggesting that EhRho1 might regulate actin filament formation in *E. histolytica* trophozoites through EhFormin1 or other effectors. Crystal structures of EhRho1 in different nucleotide states highlighted a lack of the signature Rho insert helix (7), suggesting that the EhRho1/EhFormin1 interaction might differ from that of RhoC/mDia1 (20).

In the current study, we demonstrate that EhFormin1 regulates actin polymerization through its FH2 domain. Despite considerable sequence divergence of the DAD motif and the DID motif surface expected to bind the DAD, EhFormin1 is autoinhibited by interaction between its N- and C-terminal domains. As in the case of mDia1, highly selective binding of EhRho1

to the GBD-FH3 tandem is sufficient to activate EhFormin1. Finally, a crystal structure of the EhRho1·GTPγS/EhFormin1 complex reveals a primary interface between EhRho1 and the EhFormin1 GBD with similarities to that of RhoC/mDia1. However, the absence of a Rho insert helix within EhRho1 and a large conformational difference in the DID of EhFormin1 compared to mDia1 illustrate the lack of a secondary EhRho1/EhFormin1 binding site, in contrast with mammalian homologs.

Experimental Procedures

Protein purification

EhRho1, EhRacC, EhRacD, and EhRacD were cloned from *E. histolytica* genomic DNA by PCR amplification as hexahistidine-tagged open-reading frame fusions, expressed in BL21(DE3) *E. coli*, purified by nickel affinity and gel filtration chromatography, and loaded with GTPγS as described previously for EhRho1 (7). EhFormin1 (UniProt C4M622) was cloned from genomic DNA, and fragments were PCR amplified and subcloned with a tobacco etch virus (TEV) protease-cleavable hexahistidine tag using ligation independent cloning (23). Mutagenesis was performed using the two PCR method (24). All EhFormin1 fragments were expressed in B834 *E. coli* induced with 500 μM isopropyl-β-D-thiogalactopyranoside (IPTG) for 14–16 hours at 20°C. For crystallization of the GBD-FH3 domain tandem, a selenium-containing derivative was produced by induction in minimal media containing selenomethioine (Molecular Dimensions, Apopka, FL). Bacterial cells were pelleted by centrifugation and resuspended in N1 buffer composed of 50 mM Tris pH 7.5, 250 mM NaCl, 10 mM imidazole, 1 mM DTT, and 5% (v/v) glycerol. Bacteria were lysed using pressure homogenization with an Emulsiflex (Avestin; Ottawa, Canada). Cellular lysates were cleared with centrifugation at 100,000 × *g* for 60 minutes at 4°C, and the resulting supernatant was applied to a nickel-nitrilotriacetic acid (NTA) resin FPLC column (FF HisTrap crude; GE Healthcare, Piscataway, NJ), washed with N1 buffer plus 20 mM imidazole before elution in N1 buffer with 300 mM imidazole. EhFormin1 GBD-FH3 tandem selenomethioine protein was pooled and dialyzed overnight in imidazole-free N1 buffer with His_6-TEV protease to cleave the N-terminal affinity tag. The dialysate was then passed over a second NTA column to remove TEV protease and uncleaved protein. All EhFormin1 fragments were resolved using a calibrated size exclusion column (HiLoad 16/60 Superdex 200, GE Healthcare) in S200 buffer (50 mM HEPES pH 8.0, 150 mM NaCl, and 5 mM DTT). All proteins were concentrated to 0.5 – 2 mM and snap frozen in a dry ice/ethanol bath for storage at −80°C.

Actin for *in vitro* polymerization assays was purified from rabbit skeletal muscle acetone powder as described previously (25), and further purified with gel filtration chromatography. The actin was polymerized and conjugated with pyrene as described previously (26). Following a final gel filtration step, the pyrene-actin was stored at 2 mg/mL and 4°C in G buffer (2 mM Tris pH 8.0, 0.2 mM $CaCl_2$, 0.5 mM ATP, and 5 mM DTT). Protein concentration was determined by A_{280nm} measurements upon denaturation in 8 M guanidine hydrochloride, using predicted extinction coefficients for each protein (http://us.expasy.org/tools/protparam.html).

Actin co-sedimentation

Rabbit skeletal muscle actin for co-sedimentation assays was purchased from Cytoskeleton, Inc. (Denver, CO). EhFormin1 FH2 domain and F-actin co-sedimentation assays were conducted as previously described for talin (27). Briefly, actin was diluted to 0.4 mg/mL in buffer containing 5 mM Tris pH 8.0, 0.2 mM $CaCl_2$, 0.2 mM ATP, and 0.5 mM DTT and polymerized by addition of 50 mM KCl and 2 mM $MgCl_2$, followed by incubation at room temperature for 1 hr. EhFormin1 fragments were incubated alone or with a 2:1 molar excess

of polymerized actin in binding buffer (10 mM Tris pH 7.0, 1 mM ATP, 0.2 mM DTT, 1 mM EGTA, 0.1 mM $CaCl_2$, and 2 mM $MgCl_2$) for 1 hour at room temperature. Samples were centrifuged at 100,000 × *g* and 20°C for 15 minutes. Proteins in the supernatant and pellet fractions of each experiment were resolved by SDS-PAGE and stained with Coomassie Brilliant Blue.

Actin polymerization in vitro

Monomeric pyrene-actin (~20% pyrene labeled, ~80% unlabeled) was diluted to 40 μM in buffer containing 25 μM Tris pH 7.4 and 5 mM DTT. 25 μL of diluted pyrene-actin (10 μM final concentration) and various amounts of EhFormin1 fragments and/or EhRho1 were brought to a volume of 95 μL in S200 buffer (50 mM HEPES pH 8.0, 150 mM NaCl, and 5 mM DTT). Buffer conditions were held constant in all comparison experiments, since ionic strength and pH are known to influence actin polymerization kinetics (28). Fluorescence of the pyrene moiety was monitored throughout the experiment at 30-second intervals using a FluoroLog modular spectrofluorometer (Horiba, Ann Arbor, MI) with excitation and emission wavelengths of 365 nm and 407 nm, respectively. Following establishment of a stable baseline fluorescence (~5 minutes), polymerization was initiated by addition of 5 μL polymerization buffer (1 mM Tris pH 7.4, 500 mM KCl, 20 mM $MgCl_2$, 2 mM ATP, and 5 mM DTT). Polymerization was allowed to proceed for at least 1 hour. The relative rate of polymerization was estimated by measuring the slope (fluorescence units/second) of the actin polymerization curve at 50% of the maximal fluorescent signal, as previously described (28). All slope measurements were averaged across at least 3 replicate experiments and statistical significance determined by Student's t-test.

Surface plasmon resonance

SPR-based measurements of protein-protein interactions were performed on the Biacore 3000 of UNC's Center for Structural Biology (GE Healthcare), as described previously (7). Approximately 10,000 resonance units (RUs) of purified His_6-EhFormin1 GBD-FH3 tandem and 5,000 RUs of His_6-EhFormin1 fusion were separately immobilized on a nickel-NTA biosensor chip (GE Healthcare) using covalent capture coupling as previously described (29). An empty surface served as a negative control. Experiments were performed in running buffer containing 50 mM HEPES pH 7.4, 150 mM NaCl, 0.05% NP-40 alternative (Calbiochem), 50 μM EDTA, and 1 mM $MgCl_2$. For assessment of kinetic binding properties, 3 injections of 5 μM EhRho1·GTPγS were performed at 10 μL/min with a 300 second dissociation phase. k_{obs} was obtained by fitting the average of three injections with a single phase exponential association function using GraphPad Prism v5.0. Similarly, k_{off} was obtained by fitting the average data immediately following the injections with a single phase exponential dissociation function. Since k_{obs} is dependent on the concentration of analyte, k_{on} was derived by $k_{on} = (k_{obs} - k_{off})$/(analyte concentration). An affinity constant was derived from the kinetic data by $K_D = k_{off}/k_{on}$. For equilibrium binding analyses, multiple injections were performed with increasing concentrations of GTPγS-loaded EhRho1, EhRacC, EhRacD, and EhRacG, and an affinity constant derived as described previously (7).

Crystallization and structure determination

A complex of EhRho1·GTPγS and the selenomethionine derivative of the EhFormin1 GBD-FH3 tandem (a.a. 69-418) was assembled by mixing the two proteins at a 1:1 molar ratio to a total concentration of 15 mg/mL in crystallization buffer (50 mM Tris pH 8.0, 250 mM NaCl, 2.5% (v/v) glycerol, 5 mM DTT, 50 μM GTPγS, and 1 mM $MgCl_2$) and incubation for 30 minutes at room temperature. Crystals of EhRho1·GTPγS/EhFormin1 were obtained by vapor diffusion from hanging drops at 18°C. The protein solution was mixed 1:1 with and equilibrated against crystallization solution containing 18% PEG 3350, 100 mM Tris pH

8.5, and 200 mM $MgCl_2$. Clusters of six hexagonal rod crystals grew to ~200 × 100 × 100 μm over 3 days, but diffraction was limited to >3 Å resolution. Crystal clusters were used to microseed similar crystallization experiments using the method described previously (30). Microseeded experiments yielded single hexagonal rod crystals (~300 × 150 × 150 μm) over 5 days, exhibiting the symmetry of space group $P6_1$ (a = b = 138.6 Å, c = 57.8 Å, α = β = 90°, γ = 120°) and containing one EhRho1/EhFormin1 dimer in the asymmetric unit. For data collection at 100K, crystals were serially transferred for ~1 minute into crystallization solution supplemented with 30% (v/v) glycerol in 10% increments and plunged into liquid nitrogen. Single wavelength (0.9795 Å) anomalous diffraction data were collected at the GM/CA-CAT 23-ID-B beamline at the Advanced Photon Source (Argonne National Laboratory). Data were processed using the HKL-2000 program (31). Heavy atom searching, experimental phasing, and automated model building were performed with Phenix AutoSol (32). Heavy atom searching identified 13 of 13 possible sites, and refinement yielded an estimated Bayes correlation coefficient of 51 to 2.6 Å resolution. After density modification, the estimated Bayes correlation coefficient increased to 58. ~75% of the model was constructed automatically, and the remaining portion was built manually throughout the refinement. The current model (Table 1) contains a single EhRho1/EhFormin1 dimer with EhRho1 bound to GTPγS and magnesium. Refinement was carried out against peak anomalous data with phenix.refine (32), keeping Bijvoet pairs separate, interspersed with manual model revisions using the program Coot (33). Refinement consisted of conjugate-gradient minimization and calculation of individual atomic displacement and translation/libration/screw (TLS) parameters (34). Residues 1-20 and 185-186 of EhRho1 and residues 69-72 and 378-418 of EhFormin1 could not be located in the electron density. The model exhibits excellent geometry as determined by MolProbity (35). A Ramachandran analysis of protein residue backbone angles identified 93% favored, 7% allowed, and 0% disallowed. Coordinates and structure factors are deposited in the RCSB Protein Data Bank (id 4DVG).

Results

E. histolytica Formin1 modulates actin filament formation

The Diaphanous-related formins catalyze actin polymerization through the FH2 domain (12). To examine the potential interaction of EhFormin1 with actin, two FH2 domain-containing fragments of this protein were generated and expressed from *E. coli*: FH2-DAD (a.a. 731-1182) and FH2 (731-1127) (see Figure S1). To determine whether the EhFormin1 FH2 domain interacts with actin, co-sedimentation assays were performed (27) using rabbit skeletal muscle-derived filamentous actin. The EhFormin1 fragments FH2-DAD and FH2 were highly soluble alone, but both co-sedimented with polymerized actin (Figure 1A), suggesting a direct actin/FH2 domain interaction independent of the putative DAD motif. Mutation of a conserved surface lysine (K964, Figure S2) required for actin binding by other formin FH2 domains (36) abolished actin co-sedimentation, suggesting a conserved mode of FH2 domain/actin interaction (Figure 1A). To determine whether the EhFormin1/actin interaction altered actin polymerization kinetics, *in vitro* polymerization assays were performed with pyrene fluorophore-labeled actin (~20% labeled). The FH2 and FH2-DAD fragments each decelerated actin polymerization in a concentration-dependent fashion (Figure 1B, C), as observed by the slope of the actin polymerization curve (28). Some isolated FH2 domains, such as that of Cdc12 in fission yeast, slow overall actin polymerization *in vitro* despite a positive effect on actin filament formation in a cellular context (37). Like Cdc12, the FH2 domain of EhFormin1 may cap actin filament barbed ends and require an FH1 domain-associated profilin to accelerate polymerization (38). However, no FH1 domain-containing EhFormin1 fragments could be obtained as a soluble recombinant protein from *E. coli*, precluding a direct test of this hypothesis. Relatively high

concentrations of all EhFormin1 fragments were required to significantly alter actin polymerization kinetics, likely reflecting a low affinity EhFormin1/actin interaction. Alignment of the EhFormin1 FH2 domain sequence with Diaphanous-related formins from other species (36) (28% identity and 48% similarity to yeast Bni1) indicates only moderate conservation of residues known to participate in the actin interaction (Figure S2). Similarly, the *E. histolytica* actin sequence differs significantly from rabbit skeletal muscle actin at FH2-domain interaction sites (not shown), suggesting that high EhFormin1 fragment concentrations may be required to overcome cross-species sequence and/or structural divergence.

EhFormin1 is autoinhibited by N- and C-terminal interactions

Other Diaphanous-related formins are maintained in an inactive conformation by interactions between the Diaphanous autoinhibitory domain (DAD motif) and a surface of the Armadillo repeat portion of the FH3 domain, also called the Diaphanous inhibitory domain (DID) (16, 17). Inspection of the C-terminus of EhFormin1 revealed considerable sequence divergence from the core DAD motif conserved among other known formins (MDxLLExL) (Figure 2C). Accordingly, we wondered whether the DID/DAD autoinhibitory interaction would be conserved in the case of EhFormin1. Surprisingly, the EhFormin1 FH2-DAD long fragment was seen to interact with the N-terminal GBD-FH3 domain tandem, as determined by surface plasmon resonance (Figure 2A). This intramolecular interaction required the divergent putative DAD motif, since the FH2 domain alone did not bind the GBD-FH3 domain tandem (Figure 2A,B). To determine the effects of the GBD-FH3 domain interaction on FH2 domain-catalyzed actin filament formation, *in vitro* polymerization assays were conducted in the presence or absence of a molar excess of GBD-FH3 tandem protein. Addition of the GBD-FH3 tandem selectively affected the DAD motif-containing construct, returning the rate of actin polymerization in its presence to one indistinguishable from actin alone (Figure 2D). These results suggest that the C-terminus of EhFormin1 forms a DAD motif-dependent interaction with the N-terminal GBD-FH3 domain region that prevents the modulation of actin polymerization rate by the FH2 domain.

Interaction of the EhFormin1 GBD-FH3 domain tandem with EhRho1 reverses autoinhibition of the FH2 domain

In previous work (7), we demonstrated that EhRho1 binds the GBD-FH3 domain tandem of EhFormin1 (a.a. 69-445) selectively in its GTPγS-bound, activated conformation. Since some minor degradation of that particular GBD-FH3 fragment was reported during expression and purification (*e.g.*, see Fig. 1B of (7)), we generated multiple alternative constructs containing the GBD-FH3 region, finding that amino acids 69-418 of EhFormin1 were highly stable as a recombinant protein fragment. The residues removed from this smaller fragment (*i.e.*, a.a. 419-445) correspond to the dimerization domain of mDia1 (20). The single-celled *E. histolytica* parasite expresses ~20 Rho family GTPases, raising the possibility of highly specific interactions between Rho GTPases and their signaling effectors. The EhFormin1 GBD-FH3 domain tandem (a.a. 69-418) was observed to interact selectively with EhRho1 to the exclusion of three other Rho GTPases tested (Figure 3A).

Given apparent endoproteolytic sensitivity of its unstructured, proline-rich FH1 domain, recombinant full length (and thus autoinhibited) EhFormin1 could not be produced and purified. To circumvent this problem, we produced a construct (hereafter referred to as “EhFormin1 fusion”) consisting of the N-terminal GBD-FH3 domain tandem and the C-terminal FH2-DAD fragment, connected by a 40-residue linker to simulate the presumably flexible FH1 domain (see Figure S1). While either the EhFormin1 fusion or EhRho1·GTPγS alone had no measurable effect on *in vitro* actin polymerization, the EhFormin1 fusion/EhRho1·GTPγS complex was observed to inhibit actin filament formation (Figure 3B) to a

similar degree as the corresponding FH2-DAD construct (Figure 1C). This finding suggests that EhRho1 selectively engages the N-terminus of EhFormin1, freeing the C-terminal FH2 domain to regulate actin filament formation. Using SPR, EhRho1·GTPγS was shown to bind this EhFormin1 fusion protein with ~3 μM affinity (Figure S3).

Structural features of the EhRho1/EhFormin1 complex

The sequence of the GBD-FH3 domain tandem within EhFormin1 is highly divergent compared to other known Diaphanous-related formins, with mDia1 being the closest mammalian homolog (Figure 4). EhRho1 also differs significantly from mammalian Rho GTPases and other *E. histolytica* Rho GTPases (Figure 4), particularly given its lack of a signature Rho insert helix (7). We sought a crystal structure of EhRho1 bound to EhFormin1 to allow structure-based comparison with the mammalian RhoC/mDia1 complex and to elucidate the determinants of a highly selective Rho/effector interaction. Well-diffracting crystals of EhRho·GTPγS/EhFormin1 GBD-FH3 domain tandem were obtained with aid of microseeding (see Materials and Methods). Molecular replacement attempts with structural models of either EhRho1 (PDB id 3REF) or the mDia GBD-FH3 tandem (PDB id 3EG5) did not produce electron density maps suitable for accurate modeling, likely given the divergent conformation of the GBD-FH3 domain tandem. A selenomethioine derivative of the EhFormin1 GBD-FH3 fragment was therefore generated and crystallographic phases determined by single-wavelength anomalous dispersion (SAD). For data collection and refinement statistics, see Table 1.

The overall structure of the EhRho1·GTPγS/EhFormin1 complex resembles that of human RhoC·GppNHp/mDia1 (20) except that the EhFormin1 fragment used for crystallography (a.a. 69-418) lacks the dimerization domain, and thus lacks the dimeric quaternary structure seen for mDia1 (Figure 5). The Armadillo repeats of the DID domain in EhFormin1 are rotated ~40° away from EhRho1 relative to the conformation seen in the mammalian homolog (Figure 6). EhRho1 engages the EhFormin1 GBD and the N-terminal portion of the DID Armadillo repeats through its two mobile switch regions and its α3 helix, as also seen in mammalian homologs (Figure 5). However, the GTPase binding domain of EhFormin1 differs from that of mDia by a shortened second helix and an elongated α3 helix with clearly defined and continuous electron density. As a result of a shortened α2 helix, the GBD of EhFormin1 remains farther away (~4 Å) from the putative DAD-binding site within the DID (Figure S4) which may indicate a slightly different mechanism of Rho-induced activation, since the contingently folded GBD of mDia1 is thought to contribute to DAD displacement by directly obstructing the DAD-binding site of the DID (18). EhFormin1 also has an elongated α12-α13 loop relative to mDia1 (Figure 5). This loop is near the DAD-binding site of the DID in mDia1 (18); together with the highly divergent nature of the putative DAD motif within EhFormin1 (Figure 2), the presence of this elongated loop suggests that a unique mode of DAD-mediated autoinhibition may exist in the case of EhFormin1.

The conformation of EhRho1 in the complex is nearly identical with that we have previously reported (7) of free EhRho1·GTPγS (Cα r.m.s.d. 0.4 Å, PDB id 3REG), and is also similar to RhoC in the homologous RhoC·GppNHp/mDia1 complex (Cα r.m.s.d. 1.5 Å, PDB id 1Z2C) (Figures 6, S5). The Rho insert helix of RhoC approaches the C-terminal end of the mDia1 DID (Figures 5B, 6), leading to the hypothesis that a secondary binding site (beyond the switch region/GBD interaction) may be important for mDia1 activation (14, 20). In contrast, the lack of this insert helix within EhRho1 and the relative rotation of the EhFormin1 DID indicate that such a secondary interaction is absent in the *E. histolytica* orthologues (Figures 5A, 6). An EhRho1 molecule from the adjacent asymmetric unit is interposed between the non-uniformly structured β5-α4 loop of EhRho1 and the last Armadillo repeat of the EhFormin1 DID, raising the possibility that crystal contacts could be

responsible for the rotation of the DID domain away from EhRho1 relative to the RhoC/mDia1 complex. However, this is unlikely given the large magnitude of rotation and the absence of significant contacts between the interposed EhRho1 and the DID domain; crystal contacts exist only between EhRho1 molecules in adjacent asymmetric units (see Figure S6).

The EhRho1/EhFormin1 interface is dominated by hydrophobic interactions between the two switch regions of the GTPase and the GBD (Figure 7A). The critical EhRho1 residues at this interaction site, such as Phe54 of switch 1 and Leu84 of switch 2, are conserved across the related GTPases (Figure 4A), suggesting that these hydrophobic interactions, while important for binding, do not necessarily determine the observed specificity of EhFormin1 for EhRho1. The non-conserved Asp91 of EhRho1 is positioned to potentially form ionic contacts with EhFormin1 α2 helix residues Lys108 and Lys112 (Figure 7A). The EhRho1 α3 helix contacts the first two Armadillo repeats of the EhFormin1 DID domain, primarily through residues His120 and Tyr121 (Figure 7B). The imidazole ring of His120 is oriented for a hydrogen bond interaction with Glu151 of EhFormin1. Interestingly His120 and Tyr121 are conserved in RacD, but not RacC or RacG (Figure 4A), suggesting that these two interface residues may be important for specificity. Indeed, mutation of EhRho1 His120 to Gln, the analogous residue in EhRacG, drastically reduced affinity for the EhFormin1 GBD-FH3 tandem as measured by SPR (Figure 7D). Finally, the EhRho1 switch 2 residue Arg83 is inserted into a groove between the GBD and the DID domain, a region of slightly negative charge as indicated by vacuum electrostatic calculations (Figure 7C). Arg83 is within hydrogen bonding distance to multiple exposed peptide backbone carbonyl groups in this region (Phe156 and Arg157; see Figure S7). Arg83 of EhRho1 corresponds to Arg68 of human RhoC, which engages its formin effector in a strikingly similar fashion (Figure 6B) and is required for high affinity interaction (18). However, RhoC Arg68 forms hydrogen bonds with the side chain of mDia N217 while EhRho1 Arg83 is exclusively within hydrogen-bonding distance of backbone carbonyl groups (Figure 6, S7). This arginine is also present in EhRacG, but not other Rho family GTPases (Figure 4A), implicating this particular residue as a likely determinant of specificity for the EhRho1/EhFormin1 interaction. Mutation of EhRho1 Arg83 to the corresponding Gln in EhRacC and EhRacD drastically reduced affinity for EhFormin1 (K_D >100 μM compared to ~3 μM for wild type EhRho1; Figure 7D).

Discussion

The isolated FH2 domain of EhFormin1 was observed to slow actin polymerization *in vitro*, a phenomenon also exhibited by the corresponding domain from fission yeast Cdc12 (37), suggesting a possibly similar actin barbed-end capping interaction. Other formin regions mediate interactions with proteins that can also influence its activation state as an agent of actin polymerization (39). Perhaps the best studied is the interaction of actin-bound profilin with the proline-rich FH1 domain (40). Profilins can increase the rate of actin filament elongation by formins, possibly by increasing the local concentration of actin monomers to be included in the growing filament (15). In the case of fission yeast Cdc12, the FH1 domain and associated profilin are required, in combination with the FH2 domain, for acceleration of actin polymerization (38). While *in vitro* actin polymerization assays with EhFormin1 fragments provide important mechanistic insights into activity of the isolated protein, it is important to note that the full-length protein in a cellular context is likely also modulated by subcellular localization and interactions with multiple other proteins. A limitation of the pyrene actin polymerization assay used in this study is its inability to differentiate the effects of EhFormin1 on nucleation of new actin filaments *versus* accelerated elongation of existing filaments. Nucleation and elongation are catalyzed with varying efficiency among formins (12), and further studies are thus necessary to elucidate fully the mechanisms by which EhFormin1 modulates actin polymerization.

DRFs are commonly autoinhibited by an intramolecular interaction between the N-terminal DID domain and the C-terminal DAD domain, consisting of a core MDxLLExL motif followed by a polybasic region (19). However, the C-terminus of EhFormin1 contains a highly divergent segment (MExAANxG) corresponding to the core DAD motif, suggesting a potentially unique mode of regulation. Despite poor conservation of the putative DID/DAD interface, the N- and C-terminal fragments of EhFormin1 were seen to bind one another in a DAD-dependent fashion, resulting in inhibition of FH2 domain-mediated modulation of actin polymerization. Furthermore, a fusion protein containing the N-terminal GBD-FH3 tandem and the C-terminal FH2-DAD tandem mimicked the presumably autoinhibited state of full-length EhFormin1, having no measureable effect on actin polymerization kinetics; binding of activated EhRho1·GTPγS to the GBD-FH3 region reversed the apparent autoinhibition of the EhFormin1 fusion, suggesting that the EhRho1/EhFormin1 interaction is sufficient to free the FH2 domain for modulation of actin polymerization.

The crystal structure in this study provides only the second exemplary snapshot of an interaction between a Rho GTPase and formin effector. Thus a comparison of the *E. histolytica* and human Rho/formin complexes reveals consistent structural features that are conserved across species and likely of shared importance for Rho-mediated activation of formins, as well as differences that may reflect properties of individual proteins, such as formin specificity for particular Rho GTPases. Our structural model of the EhRho1/EhFormin1 complex reveals a similar interface to that of human RhoC/mDia1 despite a distant evolutionary relationship as evidenced by substantial sequence divergence. The GTPase binding domain of EhFormin1 is quite similar to that of mDia1, with a predominant hydrophobic patch engaging the switch regions of EhRho1 (20). Arg83 of EhRho1 projects into a relatively negatively charged groove between the GBD and DID domains in a manner highly homologous to Arg68 of RhoC (20). However, the EhRho1 Arg83 residue forms hydrogen bonds exclusively with backbone carbonyl groups rather than asparagine side chains, as seen in the mammalian homolog (20). The EhRho1 switch 2 residue Arg83, together with the buried side chains of His120 and Tyr121 on the α3 helix of EhRho1, are important determinants of Rho GTPase specificity in binding EhFormin1. EhRacC and EhRacD lack the critical switch 2 arginine, while EhRacG lacks the histidine-tyrosine tandem, and all three of these Rac subfamily GTPases are unable to bind EhFormin1. Furthermore, mutation of EhRho1 residues Arg83 to the corresponding EhRacC/D glutamine or His120 to the EhRacG-like glutamine each reduced the affinity of EhRho1 for EhFormin1 by >100-fold. Such strict specificity of Rho GTPase and effector interactions is likely of particular importance in *E. histolytica* where at least 19 Rho family GTPases are apparently expressed in a single cell (7).

Several lines of evidence suggest that the mechanisms of EhFormin1 autoinhibition and its activation by EhRho1 may differ significantly from that of the well-studied mDia1 homolog (16, 17). There is poor EhFormin1 sequence conservation in the putative core DAD motif and DAD-binding surface on the DID, and EhFormin1 has a uniquely elongated α12-α13 loop near the putative DID/DAD interaction site. Furthermore, the GBD of EhFormin1 has a shortened α2 helix that would not directly obstruct the DAD-binding surface on the DID as modeled for mDia1 (Figure S4) (18). Finally, EhRho1 lacks a Rho insert helix and does not approach the C-terminus of the DID domain, indicating that a secondary EhRho1/EhFormin1 interaction between these two regions does not exist, in contrast with RhoC/mDia1.

Previous studies of EhFormin1 in the context of *E. histolytica* trophozoites (21), together with our findings ((7) and this paper), suggest that an EhRho1/EhFormin1 signaling axis may be important for formation of complex actin structures within pseudopodia and

phagocytic and pinocytic vesicles, particularly in response to extracellular cues such as serum factors. EhFormin1 also apparently exerts effects on trophozoite mitosis and cytokinesis (21). Interestingly, both EhRho1 and EhFormin1 are enriched in *E. histolytica* uropods (41), suggesting that the GTPase/effector pair may also regulate actin polymerization at the trailing edge during trophozoite migration and/or surface receptor capping critical for immune response evasion (5). Knowledge of the structural determinants defining the EhRho1/EhFormin1 interaction, and of its differences from mammalian GTPase/formin complexes (Fig. 7), should assist in understanding the contributions of this actin polymerization pathway to *E. histolytica* infectivity and invasiveness.

Supplementary Material

Refer to Web version on PubMed Central for supplementary material.

Acknowledgments

Funding Source Statement: Work in the Siderovski lab was supported by NIH grant GM082892, and DEB was supported by an individual NRSA predoctoral fellowship from the NIDDK, F30DK091978.

The authors thank the lab of Dr. Ken Jacobson (UNC) for providing pyrene-actin, Dr. John Sondek (UNC) for access to his fluorometer, and Dr. Kevin Slep and Jaime Campbell (UNC) for insights into formin-mediated cytoskeletal dynamics. We thank the UNC Center for Structural Biology for access to SPR and crystallography equipment. We also thank the Advanced Photon Source (GM/CA-CAT 23-IDB beamline) at Argonne National Labs.

Abbreviations

DID	Diaphanous inhibitory domain
DAD	Diaphanous autoinhibitory domain
FH1	formin homology 1
FH2	formin homology 2
FH3	formin homology 3
GBD	GTPase binding domain
RU	resonance unit
SAD	single-wavelength anomalous dispersion
SPR	surface plasmon resonance

References

1. Haque R, Huston CD, Hughes M, Houpt E, Petri WA Jr. Amebiasis. N Engl J Med. 2003; 348:1565–1573. [PubMed: 12700377]
2. Ravdin, JI. Amoebiasis. Vol. 2. Imperial College Press; London: 2000.
3. Voigt H, Guillen N. New insights into the role of the cytoskeleton in phagocytosis of Entamoeba histolytica. Cell Microbiol. 1999; 1:195–203. [PubMed: 11207552]
4. Guillen N. Role of signalling and cytoskeletal rearrangements in the pathogenesis of Entamoeba histolytica. Trends Microbiol. 1996; 4:191–197. [PubMed: 8727599]
5. Meza I, Talamas-Rohana P, Vargas MA. The cytoskeleton of Entamoeba histolytica: structure, function, and regulation by signaling pathways. Arch Med Res. 2006; 37:234–243. [PubMed: 16380324]
6. Lohia A, Samuelson J. Heterogeneity of Entamoeba histolytica rac genes encoding p21rac homologues. Gene. 1996; 173:205–208. [PubMed: 8964500]

7. Bosch DE, Wittchen ES, Qiu C, Burridge K, Siderovski DP. Unique structural and nucleotide exchange features of the Rho1 GTPase of Entamoeba histolytica. J Biol Chem. 2011; 286:39236–39246. [PubMed: 21930699]
8. Ridley AJ, Hall A. The small GTP-binding protein rho regulates the assembly of focal adhesions and actin stress fibers in response to growth factors. Cell. 1992; 70:389–399. [PubMed: 1643657]
9. Wennerberg K, Der CJ. Rho-family GTPases: it's not only Rac and Rho (and I like it). J Cell Sci. 2004; 117:1301–1312. [PubMed: 15020670]
10. Ghosh SK, Samuelson J. Involvement of p21racA, phosphoinositide 3-kinase, and vacuolar ATPase in phagocytosis of bacteria and erythrocytes by Entamoeba histolytica: suggestive evidence for coincidental evolution of amebic invasiveness. Infect Immun. 1997; 65:4243–4249. [PubMed: 9317033]
11. Guillen N, Boquet P, Sansonetti P. The small GTP-binding protein RacG regulates uroid formation in the protozoan parasite Entamoeba histolytica. J Cell Sci. 1998; 111(Pt 12):1729–1739. [PubMed: 9601102]
12. Chesarone MA, DuPage AG, Goode BL. Unleashing formins to remodel the actin and microtubule cytoskeletons. Nat Rev Mol Cell Biol. 2010; 11:62–74. [PubMed: 19997130]
13. Higgs HN. Formin proteins: a domain-based approach. Trends Biochem Sci. 2005; 30:342–353. [PubMed: 15950879]
14. Lammers M, Meyer S, Kuhlmann D, Wittinghofer A. Specificity of interactions between mDia isoforms and Rho proteins. J Biol Chem. 2008; 283:35236–35246. [PubMed: 18829452]
15. Schonichen A, Geyer M. Fifteen formins for an actin filament: a molecular view on the regulation of human formins. Biochim Biophys Acta. 2010; 1803:152–163. [PubMed: 20102729]
16. Nezami A, Poy F, Toms A, Zheng W, Eck MJ. Crystal structure of a complex between amino and carboxy terminal fragments of mDia1: insights into autoinhibition of diaphanous-related formins. PLoS One. 2010; 5
17. Otomo T, Tomchick DR, Otomo C, Machius M, Rosen MK. Crystal structure of the Formin mDia1 in autoinhibited conformation. PLoS One. 2010; 5
18. Lammers M, Rose R, Scrima A, Wittinghofer A. The regulation of mDia1 by autoinhibition and its release by Rho*GTP. EMBO J. 2005; 24:4176–4187. [PubMed: 16292343]
19. Nezami AG, Poy F, Eck MJ. Structure of the autoinhibitory switch in formin mDia1. Structure. 2006; 14:257–263. [PubMed: 16472745]
20. Rose R, Weyand M, Lammers M, Ishizaki T, Ahmadian MR, Wittinghofer A. Structural and mechanistic insights into the interaction between Rho and mammalian Dia. Nature. 2005; 435:513–518. [PubMed: 15864301]
21. Majumder S, Lohia A. Entamoeba histolytica encodes unique formins, a subset of which regulates DNA content and cell division. Infect Immun. 2008; 76:2368–2378. [PubMed: 18347041]
22. Ali IK, Haque R, Siddique A, Kabir M, Sherman NE, Gray SA, Cangelosi GA, Petri WA Jr. Proteomic Analysis of the Cyst Stage of Entamoeba histolytica. PLoS Negl Trop Dis. 2012; 6:e1643. [PubMed: 22590659]
23. Stols L, Gu M, Dieckman L, Raffen R, Collart FR, Donnelly MI. A new vector for high-throughput, ligation-independent cloning encoding a tobacco etch virus protease cleavage site. Protein Expr Purif. 2002; 25:8–15. [PubMed: 12071693]
24. Ho SN, Hunt HD, Horton RM, Pullen JK, Pease LR. Site-directed mutagenesis by overlap extension using the polymerase chain reaction. Gene. 1989; 77:51–59. [PubMed: 2744487]
25. Spudich JA, Watt S. The regulation of rabbit skeletal muscle contraction. I. Biochemical studies of the interaction of the tropomyosin-troponin complex with actin and the proteolytic fragments of myosin. J Biol Chem. 1971; 246:4866–4871. [PubMed: 4254541]
26. Cooper JA, Walker SB, Pollard TD. Pyrene actin: documentation of the validity of a sensitive assay for actin polymerization. J Muscle Res Cell Motil. 1983; 4:253–262. [PubMed: 6863518]
27. Srivastava J, Barber D. Actin co-sedimentation assay; for the analysis of protein binding to F-actin. J Vis Exp. 2008
28. Harris ES, Higgs HN. Biochemical analysis of mammalian formin effects on actin dynamics. Methods Enzymol. 2006; 406:190–214. [PubMed: 16472659]

29. Kimple AJ, Muller RE, Siderovski DP, Willard FS. A capture coupling method for the covalent immobilization of hexahistidine tagged proteins for surface plasmon resonance. Methods Mol Biol. 2010; 627:91–100. [PubMed: 20217615]
30. Luft JR, DeTitta GT. A method to produce microseed stock for use in the crystallization of biological macromolecules. Acta Crystallogr D Biol Crystallogr. 1999; 55:988–993. [PubMed: 10216295]
31. Otwinowski, ZaWM. Methods in Enzymology. Academic Press; New York: 1997. Processing of X-ray Diffraction Data Collected in Oscillation Mode, in; p. 307-326.
32. Adams PD, Afonine PV, Bunkoczi G, Chen VB, Davis IW, Echols N, Headd JJ, Hung LW, Kapral GJ, Grosse-Kunstleve RW, McCoy AJ, Moriarty NW, Oeffner R, Read RJ, Richardson DC, Richardson JS, Terwilliger TC, Zwart PH. PHENIX: a comprehensive Python-based system for macromolecular structure solution. Acta Crystallogr D Biol Crystallogr. 2010; 66:213–221. [PubMed: 20124702]
33. Emsley P, Lohkamp B, Scott WG, Cowtan K. Features and development of Coot. Acta Crystallogr D Biol Crystallogr. 2010; 66:486–501. [PubMed: 20383002]
34. Painter J, Merritt EA. Optimal description of a protein structure in terms of multiple groups undergoing TLS motion. Acta Crystallogr D Biol Crystallogr. 2006; 62:439–450. [PubMed: 16552146]
35. Chen VB, Arendall WB 3rd, Headd JJ, Keedy DA, Immormino RM, Kapral GJ, Murray LW, Richardson JS, Richardson DC. MolProbity: all-atom structure validation for macromolecular crystallography. Acta Crystallogr D Biol Crystallogr. 2010; 66:12–21. [PubMed: 20057044]
36. Otomo T, Tomchick DR, Otomo C, Panchal SC, Machius M, Rosen MK. Structural basis of actin filament nucleation and processive capping by a formin homology 2 domain. Nature. 2005; 433:488–494. [PubMed: 15635372]
37. Shemesh T, Kozlov MM. Actin polymerization upon processive capping by formin: a model for slowing and acceleration. Biophys J. 2007; 92:1512–1521. [PubMed: 17158576]
38. Kovar DR, Kuhn JR, Tichy AL, Pollard TD. The fission yeast cytokinesis formin Cdc12p is a barbed end actin filament capping protein gated by profilin. J Cell Biol. 2003; 161:875–887. [PubMed: 12796476]
39. Aspenstrom P. Formin-binding proteins: modulators of formin-dependent actin polymerization. Biochim Biophys Acta. 2010; 1803:174–182. [PubMed: 19589360]
40. Kursula P, Kursula I, Massimi M, Song YH, Downer J, Stanley WA, Witke W, Wilmanns M. High-resolution structural analysis of mammalian profilin 2a complex formation with two physiological ligands: the formin homology 1 domain of mDia1 and the proline-rich domain of VASP. J Mol Biol. 2008; 375:270–290. [PubMed: 18001770]
41. Marquay Markiewicz J, Syan S, Hon CC, Weber C, Faust D, Guillen N. A proteomic and cellular analysis of uropods in the pathogen Entamoeba histolytica. PLoS Negl Trop Dis. 2011; 5:e1002. [PubMed: 21483708]

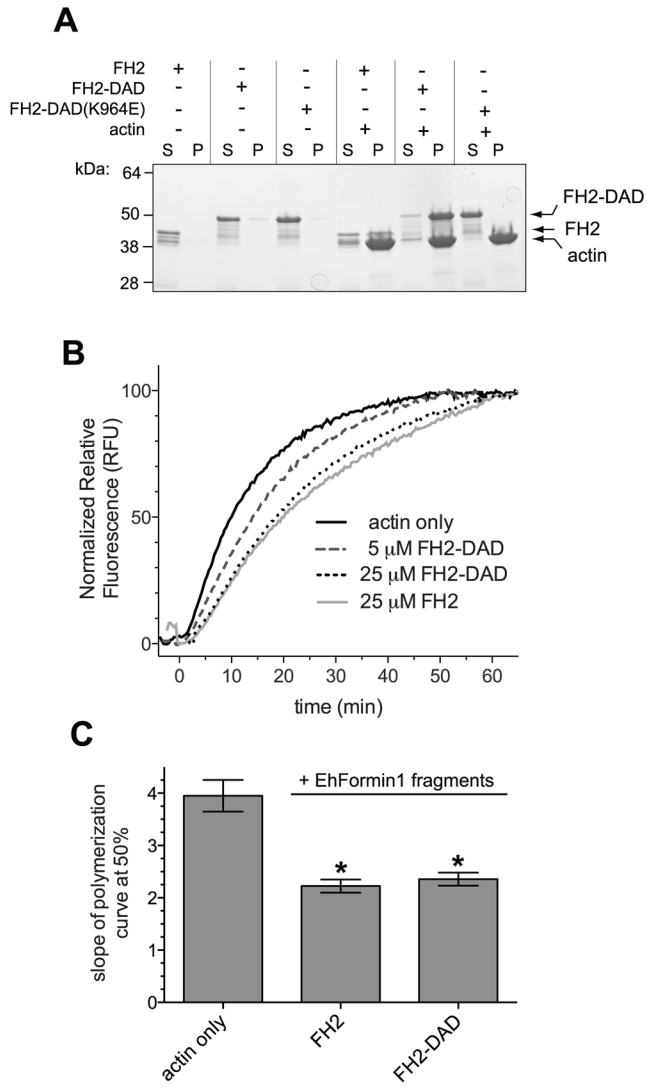

Figure 1. The FH2 domain of EhFormin1 modulates actin filament formation

A) Actin co-sedimentation assays demonstrate that the EhFormin1 FH2 domain fragment (a.a. 731-1127) and the FH2-DAD combination (a.a. 731-1182) both associate with pre-formed filamentous actin derived from rabbit skeletal muscle. Mutation of the conserved Lys964 that is critical for other formin FH2/actin interactions abolished co-sedimentation. *S* and *P* represent the soluble and pellet fractions following high-speed centrifugation, respectively. **B)** Indicated fragments of EhFormin1, each containing the FH2 domain, modulate actin polymerization *in vitro*, as measured by pyrene-actin polymerization assays. **C)** The EhFormin1 FH2 and FH2-DAD fragments are both seen to slow actin polymerization, as quantified by measuring the slope of each fluorescence curve at 50% complete polymerization. Error bars represent standard error for three or more replicate experiments. * indicates a statistically significant difference from actin only ($p < 0.05$).

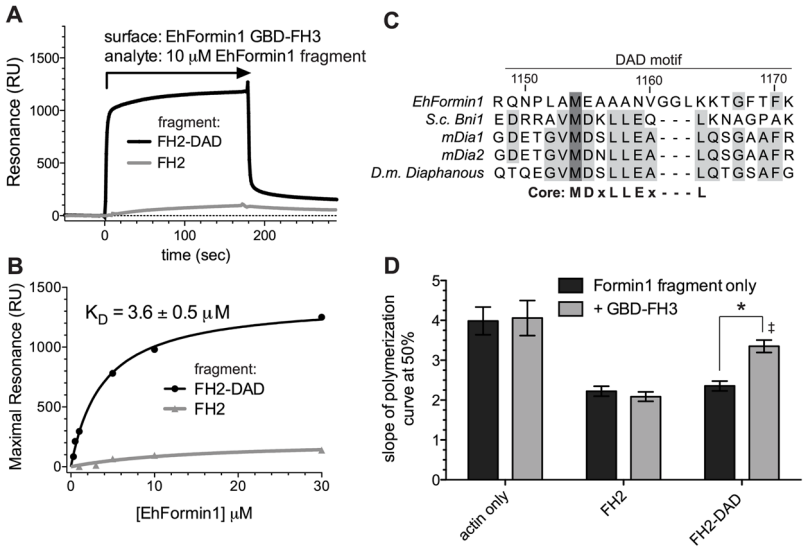

Figure 2. EhFormin1 is autoinhibited by N- and C-terminal domain interactions

A) The N-terminal GBD-FH3 domain tandem (a.a. 69-418) of EhFormin1 binds to the C-terminal FH2-DAD tandem (a.a. 731-1182), but not the FH2 domain alone (a.a. 731-1127) as determined by surface plasmon resonance. **B)** Equilibrium binding analyses revealed a DAD motif-dependent low micromolar affinity interaction with the EhFormin1 GBD-FH3 fragment. **C)** The DAD motif region, with a core motif (MDxLLExL) highly conserved among other known Diaphanous-related formins, is divergent in EhFormin1. *S.c.* indicates *Saccharomyces cerevisiae* and *D.m.* indicates *Drosophila melanogaster*, while mDia isoforms are derived from *Mus musculus*. **D)** *In vitro* actin polymerization assays indicate a DAD-motif dependent interaction between the N- and C-terminal fragments of EhFormin1 that prevents modulation of actin polymerization. Addition of a molar excess of GBD-FH3 domain tandem (100 μM) had no effect on the isolated FH2 domain from EhFormin1 or on actin alone. However, the GBD-FH3 tandem prevented deceleration of actin polymerization by the FH2-DAD fragment. Error bars represent standard error for at least 3 replicate experiments. * indicates a statistically significant difference ($p < 0.05$) and ‡ indicates an indistinguishable slope compared to actin only.

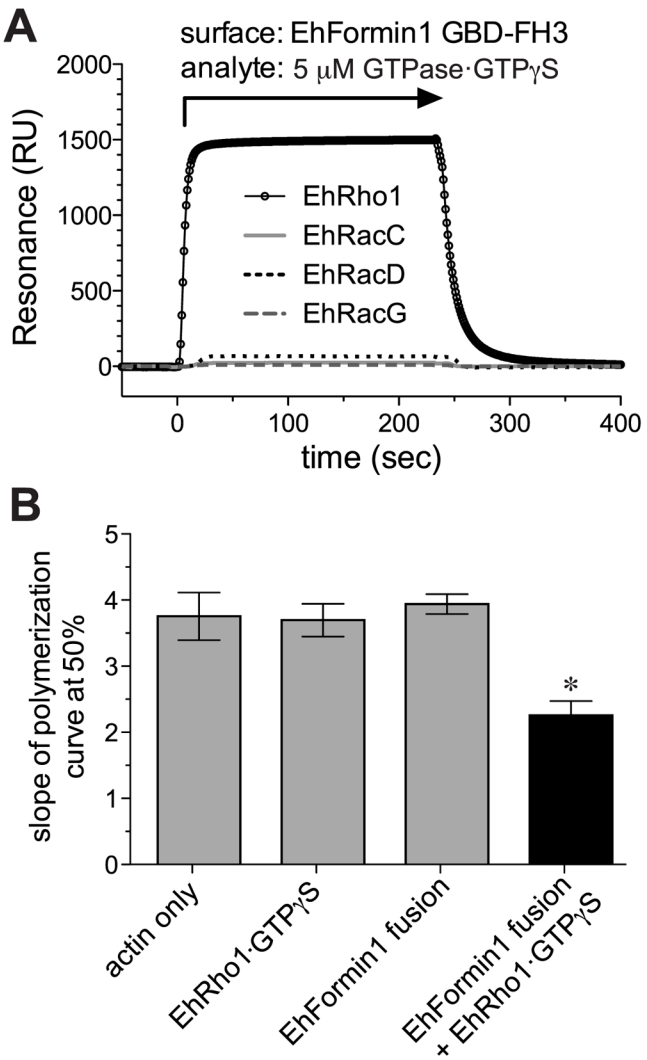

Figure 3. EhRho1 activates EhFormin1 through interaction with the GBD-FH3 domain tandem

A) The GBD-FH3 domain tandem (a.a. 69-418) of EhFormin1, immobilized on a nickel-NTA biosensor surface, selectively engaged EhRho1·GTPγS to the exclusion of multiple other Rho family GTPases from *E. histolytica*, as measured by surface plasmon resonance. **B)** The EhFormin1 fusion protein (25 μM) is apparently autoinhibited, having no measured effect on actin polymerization kinetics *in vitro*. While EhRho1·GTPγS alone (100 μM) did not perturb actin polymerization, it was capable of activating the EhFormin1 fusion, resulting in deceleration of actin polymerization comparable to that of the FH2-DAD fragment alone (Figure 1B, C). Error bars represent standard error for at least 3 replicate experiments. * indicates statistical significance ($p < 0.05$) compared to actin only.

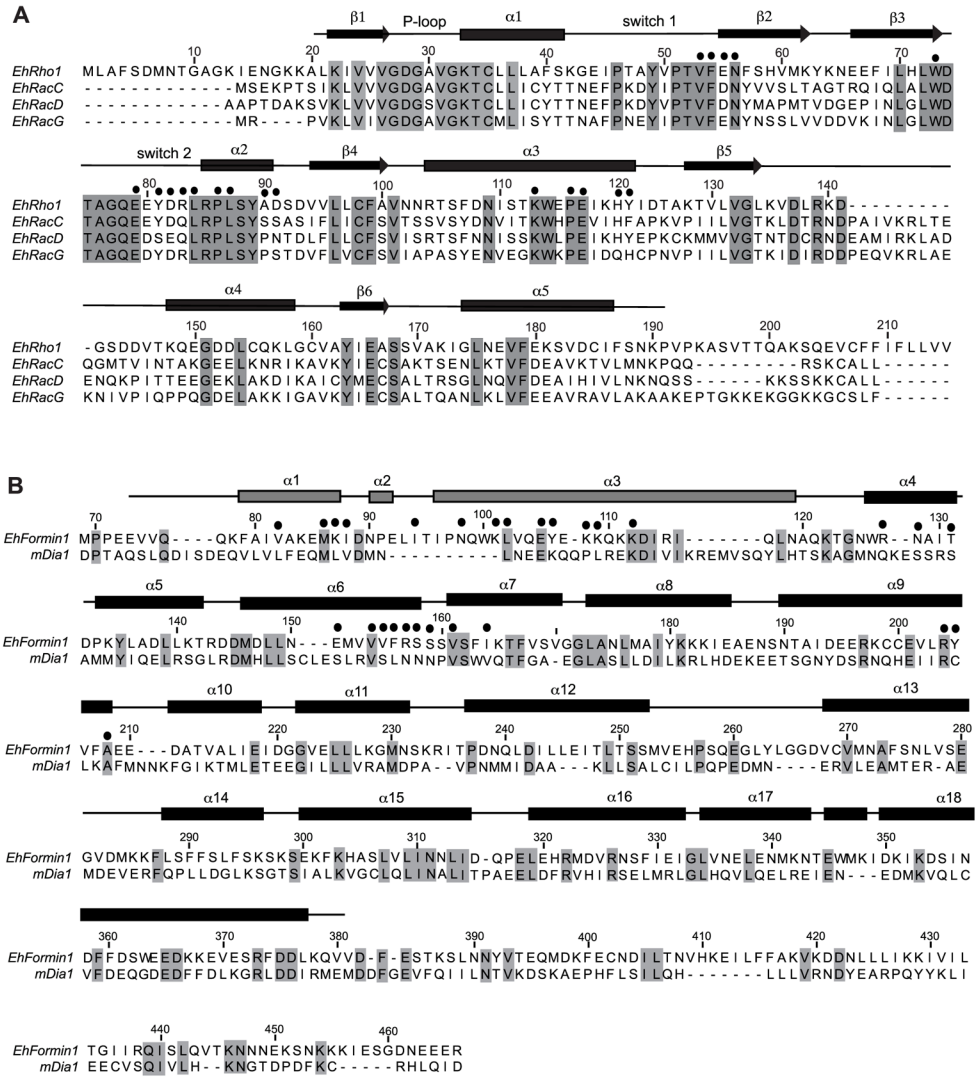

Figure 4. Sequence comparisons of Rho family GTPases and Diaphanous-related formins

A) The protein sequence of EhRho1 is aligned with three additional *E. histolytica* Rho GTPases that do not engage EhFormin1 (Figure 3A). Secondary structure from the EhRho1·GTPγS/EhFormin1 crystal structure (PDB id 4DVG; this paper) is diagrammed above the primary sequence. Black dots indicate residues of EhRho1·GTPγS within 1 Å of EhFormin1 in the complex. **B)** The protein sequence of EhFormin1 GBD-FH3 domain tandem is aligned with its closest mammalian homolog, mDia1. Secondary structure from the EhRho1·GTPγS/EhFormin1 crystal structure (PDB id 4DVG; this paper) is diagrammed above the primary sequence. Black dots indicate residues in EhFormin1 within 1 Å of EhRho1·GTPγS in the complex. All alignments were performed with ClustalW2.

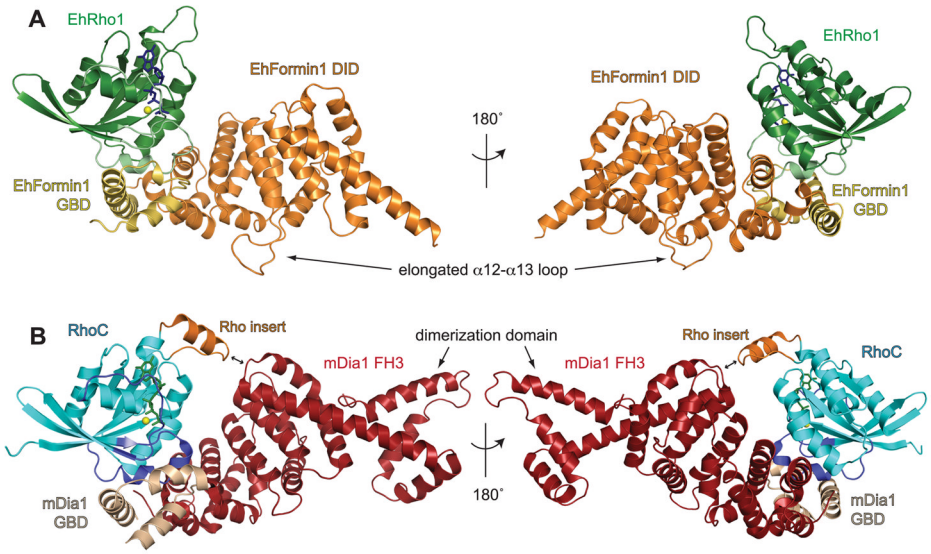

Figure 5. The crystal structure of EhRho1·GTPγS bound to the GBD-FH3 tandem of EhFormin1

A) EhRho1 (*dark green*) in its activated state bound to GTPγS (*blue sticks*) engages EhFormin1 primarily through its mobile switch regions (*light green*) and its α3 helix. The GTPase binding domain (GBD) of EhFormin1 is shown in *yellow* and the Armadillo repeats of the DID domain in *orange*. Magnesium is shown as a yellow sphere. **B)** The homologous mammalian complex between RhoC·GppNHp (*cyan*) and mDia1 (*wheat* and *red*) is posed in a similar configuration (20) (PDB id 1Z2C). EhRho1 lacks a signature Rho insert helix (highlighted in *orange* on RhoC) and the EhFormin1 DID domain Armadillo repeats are rotated away from EhRho1 relative to this mammalian complex. The EhFormin1 GBD-FH3 tandem construct used in this study also lacks the dimerization domain portion of the FH3 domain, as shown in the RhoC/mDia1 complex.

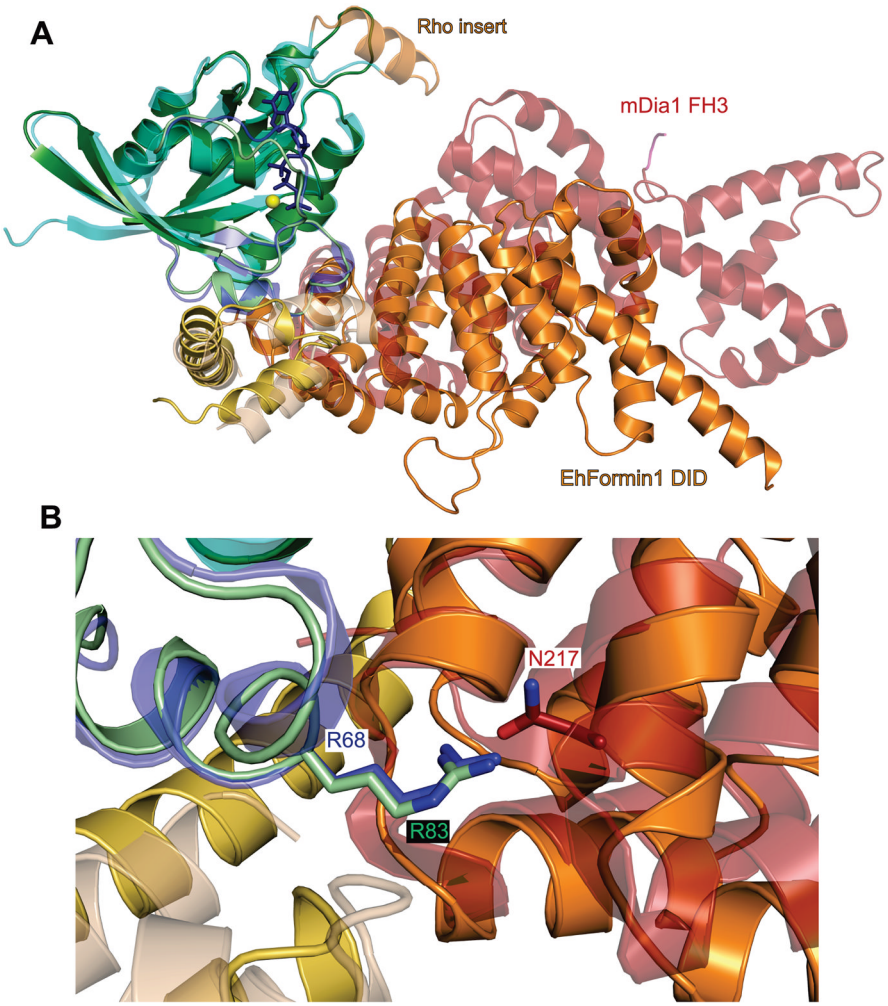

Figure 6. Structural comparison of EhRho1/EhFormin1 with mammalian RhoC/mDia1

A) The EhRho1·GTPγS/EhFormin1 complex is superimposed with RhoC·GppNHp/mDia1 (PDB id 1Z2C) using the Cα atoms of the respective Rho GTPases, and colored as in Figure 5. The Rho GTPase and GBD domains are similar across species, but the DID domain exhibits a different conformation, with an ~40° relative rotation of C-terminal Armadillo repeats. **B)** The switch 2 arginines, Arg-83 in EhRho1 and Arg-68 in human RhoC, adopt nearly identical orientations, inserting between the GBD (*yellow/wheat*) and DID domain (*orange/red*). However, Arg-68 of RhoC forms hydrogen bonds with Asn-217 of mDia1 as well as backbone carbonyl groups, while Arg-83 of EhRho1 exclusively contacts main chain carbonyl groups.

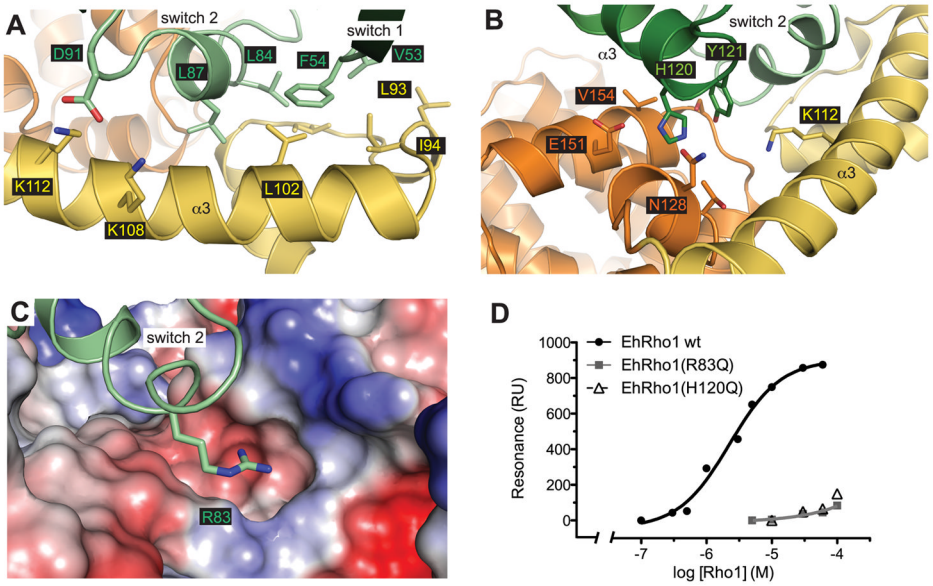

Figure 7. Structural determinants of EhRho1/EhFormin1 binding specificity

A) The EhRho1·GTPγS/EhFormin1 interface is dominated by a hydrophobic surface burial involving the switch regions of EhRho1 (*green*) and the EhFormin1 GBD (*yellow*). Key hydrophobic residues are shown in sticks. EhRho1 Asp91 is also in position to form an ionic interaction with Lys108 or Lys112 on EhFormin1. **B)** The α3 helix of EhRho1 (*green*) also contributes to the binding interface, with His120 and Tyr121 inserted between the GBD α3 helix (*yellow*) and the N-terminal portion of the DID domain (*orange*). The imidazole ring of His120 is oriented for hydrogen bonding with Glu151 of EhFormin1. **C)** EhRho1 switch 2 residue Arg83 inserts into a groove between the GBD and DID domains of EhFormin1 (shown as an electrostatic surface). The guanidinium group of Arg83 resides near an area of relative negative charge (red surface) and is within hydrogen bonding distance of multiple backbone carbonyl groups (see Figure S7). **D)** Wild type EhRho1 binds the EhFormin1 GBD-FH3 tandem, as measured by surface plasmon resonance. Mutation of either Arg83 to the corresponding glutamine in EhRacC and EhRacD or His120 to an EhRacG-like glutamine resulted in a >100-fold affinity reduction.

Table 1

Data collection and refinement statistics for the EhRho1·GTPγS/EhFormin1 complex.

	EhRho1γGTPγS/EhFormin1
PDB accession code	4DVG
Data collection	
Space group	$P6_1$
Cell dimensions	
a, *b*, *c*3(Å)	138.6, 138.6, 57.8
α, β, γ (°)	90, 90, 120
	Peak
Wavelength (Å)	0.97954
Resolution (Å)	40.0 – 2.6 (2.63 – 2.60) *
R_{merge} (%)	8.5 (58.0) **
$I/\sigma I$	15.2 (2.1)
Wilson B-factor	65.0
Completeness (%)	98.4 (86.0)
Redundancy	9.6 (6.4)
Refinement	
Resolution (Å)	35.7 – 2.6 (2.7 – 2.6)
No. reflections	19211 (2420)
Cutoff criterion	$F_{obs}/\sigma F_{obs} > 0$
R_{work}/R_{free}(%)	21.5/25.1 (33.4/37.2)
No. atoms	
Protein	3747
Ligand/ion	33
Water	4
B-factors (Å^2)	
Protein	79.5
Ligand/ion	57.4
Water	36.1
R.m.s deviations	
Bond lengths (Å)	0.010
Bond angles (°)	1.233

* Values in parentheses are for highest-resolution shell.

** All data were collected from a single crystal.